Probabilistic Neural Network and Wavelet Transform for Mapping of *Phragmites australis* Using Low Altitude Remote Sensing

Luan Casagrande and Gustavo Mello Machado
Department of Computer Engineering
Universidade Federal de Santa Catarina
Ararangua, SC, Brazil;
Email: luan.casagrande@grad.ufsc.br, g.mello@ufsc.br

Sathishkumar Samiappan, Gray Turnage,
Lee Hathcock, and Robert Moorhead
Geosystems Research Institute
Mississippi State University
Starkville, MS, USA

***Abstract*—*Phragmites australis* (common reed) commonly found in the coastal wetlands can rapidly alter the ecology of these systems by outcompeting native plant species for resources. Identifying and mapping *Phragmites* can help resource managers to restore affected wetlands. In this work, we use probabilistic neural network with wavelet texture features for mapping regions with *Phragmites* in visible spectrum imagery acquired at low altitude with small unmanned aerial system. Evaluation study was conducted with imagery acquired in the delta of the Pearl River located in southeastern Louisiana and southwestern Mississippi, United States of America. In comparison to state-of-the-art, our approach presented improvements in several statistical variables such as overall accuracy and kappa value. Furthermore, we show that the remaining omission and commission errors with this technique are generally located along boundaries of patches with *Phragmites*, which reduces unnecessary efforts for resource managers while searching for nonexistent patches.**

I. Introduction

Phragmites australis (Cav.) Trin. ex Steud. is a perennial grass species that is found on every continent except Antarctica. In the United States, it is found in the 48 contiguous states [1]. This vegetation type can grow up to 4.8 m with an average height of 3.6 m in brackish and freshwater wetlands. An invasive Eurasian haplotype of *Phragmites* has begun to proliferate in North American wetlands, often forming dense monospecific stands in invaded sites [2]. *Phragmites* invasions are frequently associated with decreases in plant biodiversity [3], declines in habitat quality for fish and wildlife [4], disruptions to biogeochemical cycles [5] and other ecosystem services. Furthermore, in highly braided waterbodies, such as the delta of the Pearl River in southeastern Louisiana, this vegetation can also be a navigation hazard to small boats by reducing visibility.

Currently, resource managers have a variety of tools to reduce or mitigate the impact of invasive *Phragmites*, including mowing, cutting, burning, grazing, and herbicides [6]. However, in order to apply such control methods, it is first necessary to map the *Phragmites* locations. Multiple methods can be used to do this, such as walking around or through a stand with a handheld Global Positioning System (GPS) unit, image acquisition by satellites, or manned aircraft. Each method has associated pros and cons.

Walking around or through *Phragmites* stand with a GPS unit to manually map the stands is labor intensive and can be dangerous to field crew members due to terrain, dense vegetation, dangerous wildlife, or insect-borne diseases. The analysis based on imagery acquired by high-resolution sensors mounted on planes or satellites can be relatively expensive [7]. Poor spatial resolution of satellite or aircraft captured imagery restricts the ability to delineate and map small *Phragmites* patches. Additionally, for free satellite imagery, rate of orbit and time to market for imagery may not be feasible for resource manager goals. Consequently, reestablishment of a *Phragmites* stands after management efforts may go unnoticed until satellite imagery is updated. Manned aircraft are an alternative to satellites, but can be prone to pilot error during image collection. Moreover, it can be costly, and may have a lower spatial resolution than what is needed.

To overcome these drawbacks, i.e., low spatial resolution and slow satellite revisit rates, we used a Low Altitude Remote Sensing (LARS) approach with a small Unmanned Aerial System (UAS). According to Anderson and Gaston [7], UASs can offer to ecologists a promising route to responsive, timely, and cost-effective monitoring of environmental phenomena at spatial and temporal resolutions that are appropriate to the scales of many ecologically relevant variables. Recently, Samiappan et al. [8] presented a method for mapping regions with *Phragmites* based on true-color high-resolution imagery acquired with UAS. Among the approaches in their investigation, they showed that the combination of Grey Level Co-Occurrence Matrix (GLCM) with Support Vector Machine (SVM) provides good results.

In this work, we present a new approach for mapping *Phragmites* using LARS. We apply, instead, wavelet transform for texture feature extraction and, based on these features, we classify regions as with or without *Phragmites* by applying Probabilistic Neural Network (PNN). Our contributions include:

- Our approach provides a decrease of 64.3% in spatial

error rate for the site I and 60.0% for site II, if compared to state-of-the-art results;
- The false positives and false negatives, with our approach, are, in general, partially true positives and true negatives, which reduces the posterior man effort while searching for inexistent patches; and
- We show the results of a comparative study about accuracy of other classification techniques;

We demonstrate the results of our work with imagery acquired by Samiappan et al. from the lower Pearl River region (see Fig. 1). The classification maps that were created using the proposed solution were validated by a domain expert.

The organization of this paper is as follows: Section II describes the main works related to mapping invasive alien plants, mainly *Phragmites*. Section III presents the details of the study area, the technical details and specifications of the UAS, and the camera sensor used. This section also covers the steps involved data preprocessing. Section IV describes the three main stages to map *Phragmites*: feature extraction, PNN training and classification process, and post-classification. Later, in section V, the results are presented followed by conclusion in Section VI.

II. Related Work

Considering that invasive plant species not only pose a serious threat to biodiversity and water resources but also have impacts on human and animal well-being [9], there is a growing community studying and discussing different approaches to map these species efficiently. *Phragmites* often spans multiple years and multiple spatial scales, from small individual patches to whole landscapes [10]. Consequently, there is a wide range of applications for mapping this specific type of vegetation considering different spatial and spectral resolutions.

One platform that is widely used to map *Phragmites* is the satellite. As already described, this kind of platform has some drawbacks if compared with other possibilities. However, generally, it can offer a higher spectral resolution that can be important to overcome the lower spatial resolution problem. In [11]–[13], the authors proposed the use of EO-1 Hyperion, Quickbird, GeoEye, and WorldView-2 platforms to remotely sense the vegetation here analyzed. Pengra et al. [11] tested the applicability of Hyperion hyperspectral satellite imagery to create a raster map of this kind of vegetation using a Spectral Correlation Mapper algorithm. The proposed solution presented limitations mainly with intermixing of different vegetation classes and the mixing of water and vegetation in deep marshess. Gilmore et al. [12] suggested the classification of few invasive plants using hierarchical object-oriented image analysis. Rules based on the spectral variability and elevation information of species throughout the growing season were used to direct classify the proposed vegetation. They used a multispectral imagery, obtained by the QuickBird satellite, and LiDAR data. This approach achieved good results with *Phragmites* mainly because of the elevation information. However, the solution had problems to classifying *Typha spp.* because this vegetation was confused with *Phragmites* and a number of species because of the diffuse clonal growth habit.

Another platform that is commonly used to acquire data and map invasive plants, is manned aircraft [13]–[15]. Calvio-Cancela et al. [14] used Ultralight Airborne Imaging Spectroscopy to map invasive plants using spectral features, sizes and growth pattern of each plant to map each area using SVM. The main problem with their solution is small patches of the target or background species, when mixed with other categories, generating mixed reflectance spectrum. Everitt and Yang [15] proposed to use aerial color-infrared (CIR) photography and CIR digital imagery combined with Iterative Self-Organizing Data Analysis that performs unsupervised classifications to map broom snakeweed. The main problem presented in their work was the similar spectral signature among different classes.

Villa et al. [13] proposed a method based on four different vegetation indexes derived from multitemporal and multisensor remote sensing dataset to monitor the conservation status and to assess the morphological complexity of *Phragmites australis*. They used data obtained through manned aerial platforms and satellites (GeoEye and Worldview 2) with spectral range from 0.40 nm to 1.04 μm. Enhanced vegetation index and normalized difference aquatic vegetation index were proved to be useful for mapping. Despite the good result presented in vegetations response in sparse to medium-density conditions, this work had a considerably high cost, mainly because of the necessity of high spatial and spectral data.

It is known that there is a growing interest in LARS approaches using UAS due to its cost, safety and better mapping capabilities. Considering this fact, recently, several works have used UAS to map *Phragmites*. In [16], Samiappan et al. used digital surface models, normalized difference vegetation index, soil-adjusted vegetation index, and morphological attribute profiles with SVM to map *Phragmites*. Zaman et al. [17] proposed the combination of high-resolution multispectral images and a classification algorithm based on learning theory to produce quantitative land cover descriptions that identify *Phragmites* locations. Husson et al. [18] considered the use of multispectral imagery as well. Their solution was based on threshold classification and Random Forest.

Despite the different classification techniques used to map *Phragmites*, the majority of the papers cited above are based on the use of sensors with a larger spectral range. This fact can be explained mainly by the fact that the relationship between Phragmites biomass and infrared/red reflectance ratios is well established in [19]. In addition, some of the authors also considered the use of elevation models, which, as already described, have a considerable capacity to distinguish a plant under analysis from other classes. The main focus of this work is to propose a novel solution based only on true-color imagery, considerably reducing the quantity of data in analyzes to generate *Phragmites* maps. In [20], a similar approach for mapping the *Phragmites* using the supervised classification was proposed. In both [8] and [20], the authors described that distortion and blurring in the imagery, and inter-mixing

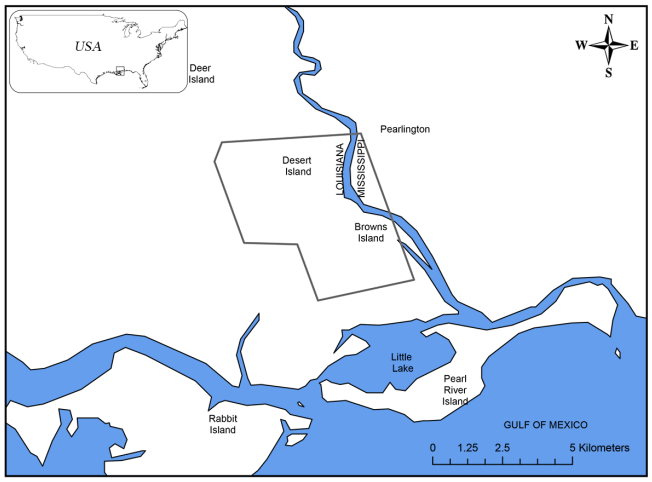

Fig. 1. The study site near Pearlington, Mississippi, USA (about 2600 acres) selected for developing and evaluating techniques to map invasive *Phragmites*.

between classes, were the main limitations of their proposed solutions. In [8], it was proposed a LARS approach using high-resolution visible imagery and texture features to map *Phragmites*. The authors showed a comparison between four techniques of texture analysis with SVM in true-color imagery to map *Phragmites*. The tests conducted with Gabor Filters (GF), GLCM, Segmentation-based Fractal Texture Analysis, and Wavelet Texture Analysis (WTA) by the authors indicated that the proposed texture-based approaches were suitable to map this kind of vegetation. This work was the most similar to the one proposed here, presenting a similar flow of execution for the generation of the map. The main differences between [8] and the work presented in this paper is the optimization of the result using PNN in place of a SVM classification.

III. Study Area

The study site near Pearlington, Mississippi, United States of America (USA) was selected for evaluating the proposed technique to map invasive *Phragmites* (Fig. 1). The region can be classified as a tidal freshwater marsh. It is one of the most intact river systems in the southeast USA [21] with one of the healthiest marsh complexes in the USA [22]. The Pearl River has been identified as a high priority focus for conservation attention within the Eastern Gulf Coastal Plain and Northern Gulf of Mexico eco-regions [22]. Data was collected on 23 September 2014 in the lower Pearl River basin west of Pearlington, Mississippi north and south of US Highway 90. Analysis was conducted on data collected at two sites: (I) Desert Island and (II) Browns Island, with a total area of approximately 2600 acres (1063 ha).

A. Image Aquisition

The data was acquired using a waterproof Altavian Nova UAS that weighs approximately 7 kg with payload, has an 2.7 m wingspan and 1.5 m length, and is capable of water landings. This system can capture data on flights lasting 90 minutes.

The camera used to acquire images is a modified Canon Rebel EOS SL1 that captures true color images. The size of the images acquired is 5184×3456 pixels with 8 bits per RGBA channel. Considering the camera's specifications and an altitude of approximately 231m, the ground sample distance maintained was approximately 5 cm/pixel side. Aiming to keep an overlap of five images or more in the region of analysis, the flight plan was defined considering 50% side overlap and 70% forward overlap.

The software used to create the mosaic was Agisoft Photoscan Pro. The latitude, longitude, and altitude that the UAS stored during the flights were used to define initial camera positions in the software. Orthomosaic tiles were exported at a size of 3184×3184 pixels and stitched together into a virtual mosaic using Geospatial Data Abstraction Layer software. The geo-referencing was performed using only data obtained through the flight telemetry data.

B. Ground Reference Map

To build the ground reference map (GR), in the work by Samiappam et al. [8], domain experts recorded the boundaries of three selected patches by walking around them with a Trimble Geo 7X GPS unit, with sub-decimeter accuracy. After collecting coordinates of GR patches, the true color image was loaded into Environmental Systems Research Institute ArcMap program. The boundaries of the same three patches were manually digitized by a domain expert based on direct visual inspection of the image mosaic in ArcMap. These digitized boundaries were then compared to the in situ patch GR boundaries. Samiappan et al. showed that the difference between both boundaries is almost insignificant. Aiming to physically verify the rest of the GR *Phragmites* patch locations along river channels and roadways, the authors of this work returned to the field. The authors navigate around these patches with a GPS unit or visit patches that were inland from a river channel or roadway during the revisit. These series of actions were performed with the intention of ensuring that the digitized boundaries could be used as a ground reference to verify the system's accuracy.

IV. Mapping *Phragmites*

Our approach can be divided in three stages: texture feature extraction, PNN classification, and Post-classification.

The input to our classification system consists of a true-color image in GeoTIFF format, that provides extra georeferencing information. In our study, one pixel of such images represents a square area of approximately $25cm^2$. We divide the input images into blocks of 100×100 pixels to further perform classification of blocks individually. Thus, we classify blocks with physical area of ca. $25m^2$ as with *Phragmites* or without *Phragmites*. This setup was defined aiming to respect the ability of the system to delimit and map small *Phragmites* patches.

A. Wavelet Texture Features Extraction

Samiappan et al. [8] reported that, in imagery captured with UAS, *Phragmites* are visually distinguishable from other

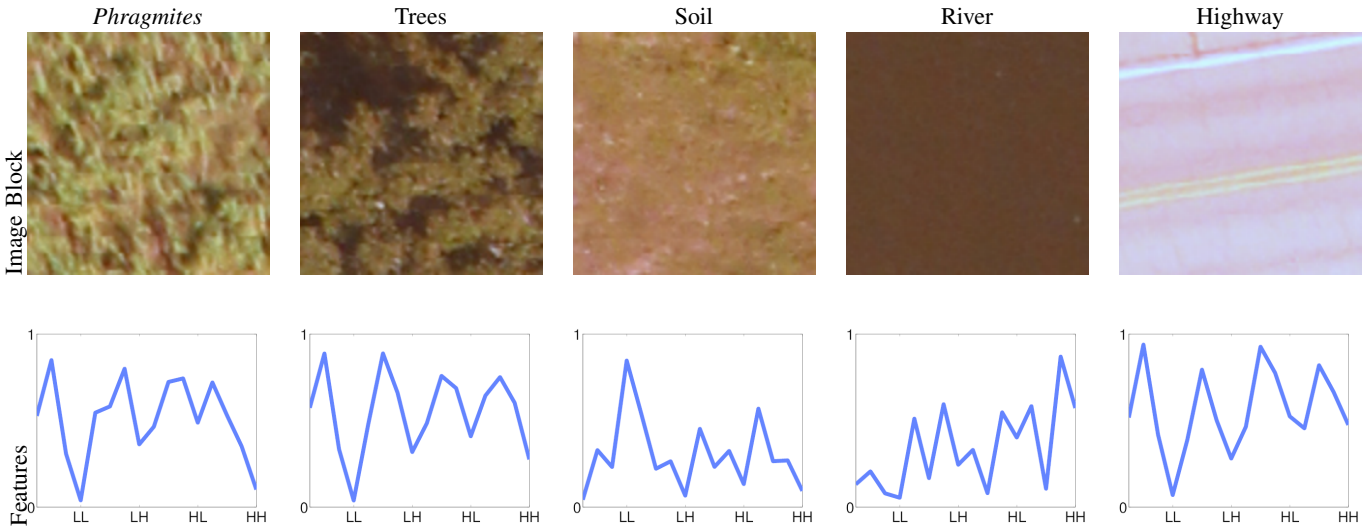

Fig. 2. Image blocks examples (top), representing the five most common object categories in the study area, and their respective wavelet texture signatures (bottom) concerning four statistical properties (mean, entropy, standard deviation, and energy value) for each sub-band (LL, LH, HL, and HH). For illustration purpose the values were normalized.

objects due to unique properties like roughness, granulation, and regularity. In Fig. 2 (top), a set of blocks representing areas with *Phragmites*, trees, soil, river, and highway, let us compare and notice these characteristics. Hence, at least visually, we can identify blocks with *Phragmites* due to their spatial frequency distribution.

Human visual system is very effective at interpreting spatial frequency of the luminance channel at multiscale. This ability can be emulated by means of wavelet transforms. Wavelet transforms enable multi-resolution analysis of features by decomposing data $X = \{x_1, x_2, ..., x_N\}$ into two sub-bands $L|H = \{l_1, l_2, ..., l_{\frac{N}{2}}, h_1, h_2, ..., h_{\frac{N}{2}}\}$, where L represents the low-pass component and H represent its high-pass counterpart. This can be extended to bi-dimensional data, where four sub-bands are obtained by performing low- and high-pass decomposition in both horizontal and vertical directions. In this work, each input block is converted to grayscale by computing the luminance and after, the blocks are applied to the Haar wavelet transform [23], that extracts the low-pass components by averaging and the high-pass counterpart by differencing, according to the following equations:

$$l_i = \frac{x_{2i} + x_{2i+1}}{2} \tag{1}$$

$$h_i = \frac{x_{2i} - x_{2i+1}}{2} \tag{2}$$

For such, we employ a first pass horizontally to the image block, dividing it into two subregions concerning the two sub-bands L (low-frequency) and H (high-frequecy). Later, we take these sub-bands as input to a second pass, now vertically, which results in four sub-bands with 2:1 downsampling. Fig. 3b shows the four sub-bands (i.e., approximation LL, details in horizontal point LH, details in vertical point HL, and details in diameter HH at top-left, top-right, bottom-left, and bottom-right, respectively) obtained after applying one level Haar wavelet transform to Fig. 3a. The input images were captured at an approximate constant and low ground distance by the UAS, thus, more than one level Haar transform is not required.

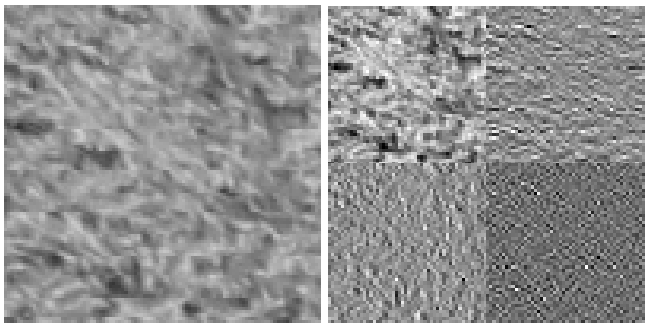

(a) (b)

Fig. 3. One level of Haar wavelet transform applied to (a) example block with 100×100 pixels. The output (b) is divided into four sub-regions with 50×50 pixels each. Top-left (LL) shows the approximation values, top-right (LH) shows details in horizontal, bottom-left (HL) shows details in vertical, and bottom-right (HH) shows details in diagonal.

In order to represent spatial frequency, from each sub-band, we compute four statistical parameters, i.e., mean, standard deviation, entropy (S), and energy value (E), composing 16 parameters of each image block. Entropy is often described as a measure of randomness and energy a measure of frequency distribution. Entropy and energy can be computed as follows:

$$S = -\sum_i p_i \log p_i, \tag{3}$$

$$E = \sum_i |p_i|^2, \tag{4}$$

where p_i are pixels' values. Fig. 2 (bottom) shows the values of these four parameters for the example blocks on the top

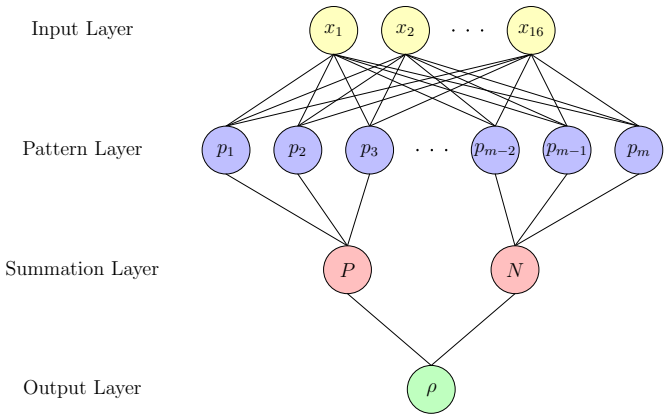

Fig. 4. Illustration of our PNN's architecture for classification. The input layer has 16 nodes, one for each input parameter. The pattern layer is fully connected to the input layer, and its nodes represent the training cases. The summation layer averages the results from pattern layer for each of the two categories (positive P or negative NP). And the output layer decides to which category (i.e., with or without *Phragmites*) the input corresponds.

row. Note the difference in the values of parameters for each block category, which makes these parameters suitable for classification of *Phragmites* in this context.

B. Classification with Probabilistic Neural Networks

Specht [24] presented the PNN classifier, that is a specific configuration of feedforward artificial neural network (ANN). According to Specht, there are some advantages in using PNN over other classification algorithms, among them, it has a well-defined structure and, hence, straightforward implementation; it has an instantaneous training process, where the training cases are incorporated into the network as new nodes; and it is robust with respect to noise in the input. Moreover, under certain easily met conditions, it can approach a Bayes optimal result.

A typical PNN has four layers: input, pattern, summation, and output (Fig. 4). The input layer maps the n input parameters from the input data to the PNN. We represent this layer as the vector v with length $n = 16$, where each input node x_i corresponds to one component of v, in our case, the four parameters computed from each sub-band in the input block.

The pattern layer has one node p_i for each training case and it is fully connected with the input layer. Computation in each pattern node is given due to the following equation:

$$p_i = \frac{1}{(2\pi)^{\frac{n}{2}}\sigma^n} exp\left[-\frac{(v-v_i)^T(v-v_i)}{2\sigma^n}\right], \qquad (5)$$

where v_i is the vector representing the corresponding training case and σ is a smoothing parameter, experimentally defined here as $\sigma = 0.1$.

Note that the pattern nodes can be divided into subgroups according to the training cases' category. In this work, it was defined two categories in the PNN: positive answer (P) for blocks with *Phragmites* and negative answer (NP) for blocks without *Phragmites*.

The summation layer computes the maximum likelihood of input v being classified into each one of the categories. For such, each node in the summation layer corresponds to one distinct category and it is connected to the corresponding subgroup of nodes in the pattern layer. In fact, the summation nodes perform an averaging of the results in the connected pattern nodes as follows:

$$s_c = \frac{1}{N_c}\sum_{i}^{N_c} p_i \qquad (6)$$

where p_i in the sum represents the results from pattern nodes of category c and N_c is the total number of pattern nodes in this category. If the probabilities for each category are the same, the decision layer unit classifies the pattern v following the Bayes' decision rule based on the output of all summation layer neurons as follows:

$$\hat{C}(v) = argmax\left\{s_c\right\},\ i = 1, 2, \cdots, q \qquad (7)$$

Where $\hat{C}(v)$ denotes the estimated class of the pattern w and q is the total number of classes in the training samples.

Prior to running the PNN, it is necessary to define the training cases. For such, we use a ground reference map that indicates the regions with *Phragmites* in the input map. The training cases are randomly selected blocks, where 50% of them are completely inside regions with *Phragmites* and the other half are completely outside these regions. The total number of selected blocks comprises ca. 10% of the whole input map area. The remaining blocks, which are not known by the classifier, were used for the system evaluation. With the training and test set defined, the system was trained and the classes were predicted.

C. Post-Classification

After the PNN classification, the maps are generated using the cartography information from the imagery. To do this, a binary image was constructed where each block of 100×100 pixels is defined with the respective class value. After, the perimeter of each *Phragmites* patch is identified and the positions in the perimeter image are transformed in latitude and longitude using the image properties and cartographic information saved. The perimeter of all *Phragmites* patches is then used to create a shape file. This final georeferenced map can be easily utilized by the resource manager for decision making.

V. Results

To evaluate the system's performance we used the kappa coefficient (κ), overall accuracy (OA), agreement (A), commission error (CE), and omission error (OE). According to Viera and Garrett [25], the κ is the most commonly used statistic in remote sensing for studies that measure agreement between two or more learners. The OA is the rate of correct pixels among all pixels. The A is the rate of correct pixels within a given category, in other words, it represents the probability of a reference pixel being correctly classified. The

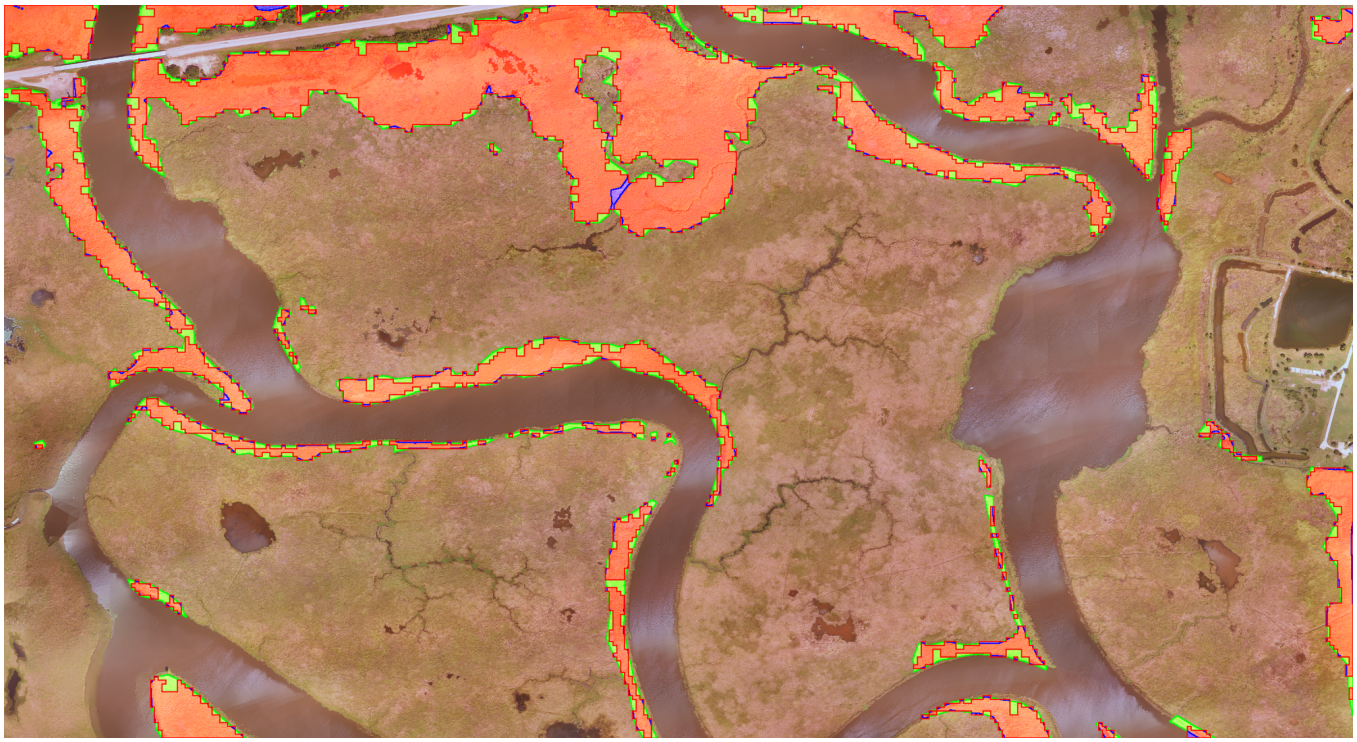

Fig. 5. Classification results obtained using PNN with Wavelet textures for study site I, where *Phragmites* agreement is outlined in red, omission cases outlined in green, and commission cases in blue.

Fig. 6. Classification results obtained using PNN with Wavelet textures for study site II, where *Phragmites* agreement is outlined in red, omission cases outlined in green, and commission cases in blue.

CE is the rate of pixels misclassified as P, and the OE is the rate of pixels misclassified as NP.

Table I shows the statistical results for our approach. Note that the κ values are all above 0.8, which, according to [25], represents substantial to almost perfect agreement. Furthermore, the OE is substantially higher than the CE for P answers. There are several factors that explain these values, for example, it is possible to establish that, with our approach, the main area of misclassification is with respect to blocks that represent locations of transition between P and NP (see Fig. 5 and 6). In some of these blocks the non-*Phragmites* object comprises higher area than *Phragmites*, and, as consequence, the distance found by the classifier between the block's parameters and NP was smaller than with P. Another source of errors are plant species of interest intermixed with other species. Again, it is possible that these other species are more representative in the block being analyzed, and thus, the PNN classifier will identify as NP.

TABLE I
CLASS-SPECIFIC CLASSIFICATION ACCURACIES (IN PERCENTAGE), AGREEMENT (IN PERCENTAGE), OA (IN PERCENTAGE), AND KAPPA STATISTIC FOR SITE I AND II.

	Site I		Site II	
Class	P	NP	P	NP
OE (%)	14.8	0.4	20.6	0.2
CE (%)	3.1	2.4	3.8	1.6
A (%)	85.2	99.6	79.3	99.8
κ	0.89		0.86	
OA (%)	97.5		98.3	

Based on the work by Kotsiantis [26], we performed a comparative study with other classification approaches. Since decision trees can be translated into a set of rules by creating a separate rule for each path [27], this study did not consider this kind of logical learning method. In addition, since we propose the use of PNN and WTA for mapping *Phragmites*, and PNN is a specific configuration of ANN, we did not include other neural networks for comparison. Hence, our comparative study comprises the following classifiers: SVM, k-nearest neighbors (k-NN), Decision Tree (DT), and Nave Bayes (NB). Tables II and III show the system's performance considering these classifiers for site I and II, respectively. The results for SVM were obtained from the work by Samiappan et al. [8].

From the data presented in Tables I, II, and III, it is possible to conclude that there is an inverse relationship between *Phragmites* and not *Phragmites* agreement. While k-NN and DT have higher P agreements, they have smaller NP agreements. In the other side, PNN and SVM have higher NP agreements and smaller P agreements. Despite de fact that PNN did not present the highest *Phragmites* agreement, it presented the highest not *Phragmites* agreement, κ, and OA for both sites. Among all, k-NN presented the highest P agreement and SVM the highest OA for both sites.

TABLE II
LEARNING ALGORITHMS ASSESSMENTS FOR SITE I

	SVM		k-NN		DT		NB	
Class	P	NP	P	NP	P	NP	P	NP
OE (%)	27.0	2.6	7.7	7.4	12.8	6.7	10.4	11.1
CE (%)	17.9	4.3	32.3	1.4	31.4	2.3	42.5	1.9
A (%)	72.9	97.3	92.3	92.6	87.2	93.3	89.6	88.9
κ	0.73		0.74		0.72		0.64	
OA (%)	93.0		92.6		92.4		89.0	

TABLE III
LEARNING ALGORITHMS ASSESSMENTS FOR SITE II

	SVM		k-NN		DT		NB	
Class	P	NP	P	NP	P	NP	P	NP
OE (%)	35.6	1.3	10.0	7.7	12.4	9.5	24.6	9.7
CE (%)	16.5	3.6	45.54	1.1	51.4	1.4	55.6	2.7
A (%)	64.4	98.7	90.0	92.3	87.6	90.5	75.4	90.3
κ	0.70		0.64		0.57		0.5	
OA (%)	95.5		92.1		90.2		89.0	

In addition, if we compare the most reliable maps from site I, i.e., PNN (Fig. 5), SVM (see [8]), and k-NN (Fig. 7), it is possible to verify that PNN was the unique technique that did not present new *Phragmites* patches that don't exist. That is, the system's misclassification were mainly located in the boundaries, and, in few cases, in the middle of real patches. Note that, misclassification along boundaries will not increase resource managers' effort, since they would not need to move to new areas that do not have *Phragmites*. Thus, the proposed solution improves the confidence level of the generated maps.

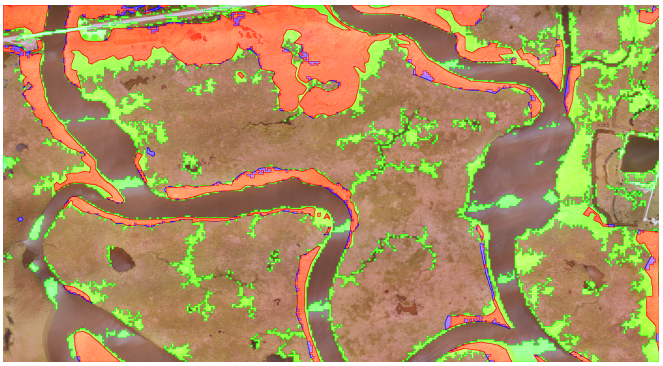

Fig. 7. Site I assessment for k-NN classification, where *Phragmites* agreement is outlined in red, omission cases outlined in green, and commission cases in blue.

A. Implementation Details

The experiments were performed on a 2.5GHz Intel i5-2450M on 64-bit Microsoft Windows operating system with 8 GB of RAM. The overall processing time per square kilometer is approximately 45 min. The proposed solution was developed using MATLAB.

VI. CONCLUSION

We presented a novel approach for automatic classification of invasive *Phragmites* in imagery aquired by LARS with a small, hand-launched UAS. For comparison and consistency, we performed evaluation with the same imagery aquired by Samiappan et al. [8]. Our experimental study shows that the combination of PNN and wavelet textures yields superior classification accuracies if compared to that of SVM, k-NN, DT, and NB. A major improvement in class accuracies was found with the reduction of OEs and CEs for both P and NP classes with misclassification generaly along boundaries of *Phragmites*' patches. Moreover, our approach improves the κ accuracies, with values above 0.8.

The ground reference data used to assess the accuracy of the proposed classification scheme is a combination of field visits, photographs and visual analysis of the high-resolution LARS-UAS data by an expert in the field of aquatic invasive species. In numerous inaccessible parts of the study areas, other native and non-native trees were surrounded by dense stands of *Phragmites*, which resulted in the assumption that the entire area was *Phragmites*. The resulted OE caused by this disagreement was found to be approximately equal to 50% of total CE. A significant amount of OE and CE was reduced with the application of PNN without adding any other information such as other spectral bands.

Based on experimental results presented in this research, wavelet texture features are able to distinguish *Phragmites* stands accurately. Experimental results reporting κ, OA, OE, and CE are sufficient to conclude that low-cost UAS based mapping can be achieved with a visible range sensor and LARS.

As future work, we propose to reduce the computational cost with a General-purpose Graphics Processing Unit (GPGPU)

implementation of both, wavelet texture features extraction and classification with PNN. In addition, aiming to reduce the *Phragmites* omission error, we propose the implementation of recursive block subdivision and further classification when the original block summation is below a specific threshold.

ACKNOWLEDGMENT

The authors would like to thank Michael Braswell, Ashley Kosturock, and Hunter Rawson from Mississippi State University for assisting with data collection, as well as Kevin Choate and Allan Austria from Altavian for their assistance with the UAS.

REFERENCES

[1] R. J. Marks M, Lapin B, "Phragmites australis (p. communis): threats, management and monitoring," Natural Areas Journal, p. 285294, 1994.

[2] K. Saltonstall, "Cryptic invasion by a non-native genotype of the common reed, phragmites australis, into north america," Proceedings of the National Academy of Sciences, vol. 99, no. 4, pp. 2445–2449, feb 2002.

[3] M. D. Bertness, P. J. Ewanchuk, and B. R. Silliman, "Anthropogenic modification of new england salt marsh landscapes," Proceedings of the National Academy of Sciences, vol. 99, no. 3, pp. 1395–1398, jan 2002.

[4] R. M. Chambers, L. A. Meyerson, and K. L. Dibble, "Ecology of phragmites australis and responses to tidal restoration," in Tidal Marsh Restoration. Island Press/Center for Resource Economics, 2012, pp. 81–96.

[5] L. A. Meyerson, R. M. Chambers, and K. A. Vogt, "The effects of phragmites removal on nutrient pools in a freshwater tidal marsh ecosystem," Biological Invasions, vol. 1, no. 2/3, pp. 129–136, 1999.

[6] E. L. G. Hazelton, T. J. Mozdzer, D. M. Burdick, K. M. Kettenring, and D. F. Whigham, "Phragmites australis management in the united states: 40 years of methods and outcomes," AoB Plants, vol. 6, no. 0, pp. plu001–plu001, jan 2014.

[7] K. Anderson and K. J. Gaston, "Lightweight unmanned aerial vehicles will revolutionize spatial ecology," Frontiers in Ecology and the Environment, vol. 11, no. 3, pp. 138–146, apr 2013.

[8] S. Samiappan, G. Turnage, L. Hathcock, L. Casagrande, P. Stinson, and R. Moorhead, "Using unmanned aerial vehicles for high-resolution remote sensing to map invasive Phragmites australisin coastal wetlands," International Journal of Remote Sensing, pp. 1–19, oct 2016.

[9] D. Pimentel, R. Zuniga, and D. Morrison, "Update on the environmental and economic costs associated with alien-invasive species in the united states," Ecological Economics, vol. 52, no. 3, pp. 273–288, feb 2005.

[10] E. Adam, O. Mutanga, and D. Rugege, "Multispectral and hyperspectral remote sensing for identification and mapping of wetland vegetation: a review," Wetlands Ecology and Management, vol. 18, no. 3, pp. 281–296, dec 2009.

[11] B. W. Pengra, C. A. Johnston, and T. R. Loveland, "Mapping an invasive plant, phragmites australis, in coastal wetlands using the EO-1 hyperion hyperspectral sensor," Remote Sensing of Environment, vol. 108, no. 1, pp. 74–81, may 2007.

[12] M. S. Gilmore, E. H. Wilson, N. Barrett, D. L. Civco, S. Prisloe, J. D. Hurd, and C. Chadwick, "Integrating multi-temporal spectral and structural information to map wetland vegetation in a lower connecticut river tidal marsh," Remote Sensing of Environment, vol. 112, no. 11, pp. 4048–4060, nov 2008.

[13] P. Villa, A. Laini, M. Bresciani, and R. Bolpagni, "A remote sensing approach to monitor the conservation status of lacustrine phragmites australis beds," Wetlands Ecology and Management, vol. 21, no. 6, pp. 399–416, jul 2013.

[14] M. Calviño-Cancela, R. Méndez-Rial, J. Reguera-Salgado, and J. Martín-Herrero, "Alien plant monitoring with ultralight airborne imaging spectroscopy," PLoS One, vol. 9, no. 7, p. e102381, jul 2014.

[15] J. H. Everitt and C. Yang, "Mapping broom snakeweed through image analysis of color-infrared photography and digital imagery," Environmental Monitoring and Assessment, vol. 134, no. 1-3, pp. 287–292, feb 2007.

[16] S. Samiappan, G. Turnage, L. A. Hathcock, and R. Moorhead, "Mapping of invasive phragmites (common reed) in gulf of mexico coastal wetlands using multispectral imagery and small unmanned aerial systems," International Journal of Remote Sensing, pp. 1–22, dec 2016.

[17] B. Zaman, A. M. Jensen, and M. McKee, "Use of high-resolution multispectral imagery acquired with an autonomous unmanned aerial vehicle to quantify the spread of an invasive wetlands species," in 2011 IEEE International Geoscience and Remote Sensing Symposium, July 2011, pp. 803–806.

[18] E. Husson, F. Ecke, and H. Reese, "Comparison of manual mapping and automated object-based image analysis of non-submerged aquatic vegetation from very-high-resolution UAS images," Remote Sensing, vol. 8, no. 9, p. 724, sep 2016.

[19] M. Ihse and W. Graneli, "Estimation of reed (phragmites australis) biomass through spectral reflectance measurements," Biomass, vol. 8, no. 1, pp. 59–79, jan 1985.

[20] H. Brooks, "Exotic vegetation assesment (eva): Remote sensing phragmites australis at presque isle state park," Master's thesis, The Pennsylvania State University Schreyer Honors College, 2014.

[21] E. G. C. P. C. Team, "East gulf coastal plain ecoregional plan. volume i and ii (revision)," The Nature Conservancy, Arlington, Virginia, Tech. Rep., 2001.

[22] D. Bird and A. S. Kyle, "Conservation area plan for the pearl river," Louisiana Department of Environmental Quality, CFMS Cooperative Agreement No. 583066, Tech. Rep., August 2004.

[23] R. S. Stanković and B. J. Falkowski, "The haar wavelet transform: its status and achievements," Computers & Electrical Engineering, vol. 29, no. 1, pp. 25–44, jan 2003.

[24] D. F. Specht, "Probabilistic neural networks," Neural Netw., vol. 3, no. 1, pp. 109–118, Jan. 1990.

[25] A. J. Viera and J. M. Garrett, "Understanding interobserver agreement: The kappa statisti," Journal of Family Medicine, pp. 360–363, may 2005.

[26] S. B. Kotsiantis, "Supervised machine learning: A review of classification techniques," in Proceedings of the 2007 Conference on Emerging Artificial Intelligence Applications in Computer Engineering: Real Word AI Systems with Applications in eHealth, HCI, Information Retrieval and Pervasive Technologies. Amsterdam, The Netherlands, The Netherlands: IOS Press, 2007, pp. 3–24.

[27] J. R. Quinlan, C4.5: Programs for Machine Learning. San Francisco, CA, USA: Morgan Kaufmann Publishers Inc., 1993.